High-Performance Electrocatalysts for Oxygen Reduction Derived from Polyaniline, Iron, and Cobalt

Gang Wu, *et al.*

Science **332**, 443 (2011);
DOI: 10.1126/science.1200832

reaction of an organometallic reagent at a specific position, usually ortho to the directing group, followed by the reaction of the metallated aromatic compound with an electrophile. For application of these groups in directed *ortho*-lithiation see (*31*).
8. P. N. Rylander, *Hydrogenation Methods* (Academic Press, London, 1985), pp. 157–163.
9. M. K. Huuska, *Polyhedron* **5**, 233 (1986).
10. S. Utoh, T. Hirata, H. Oda, C. Yokokawa, *Fuel Proc. Tech.* **14**, 221 (1986).
11. E. M. Van Duzee, H. Adkins, *J. Am. Chem. Soc.* **57**, 147 (1935).
12. G. Stork, *J. Org. Chem.* **69**, 576 (1947).
13. A. Maercker, *Angew. Chem. Int. Ed. Engl.* **26**, 972 (1987).
14. P. Dabo, A. Cyr, J. Lessard, L. Brossard, H. Ménard, *Can. J. Chem.* **77**, 1225 (1999).
15. Stoichiometric hydrogenolysis of aromatic C-O bond in a palladium pincer complex was reported in (*32*).
16. P. J. Dyson, *Dalton Trans.* 2964 (2003).
17. E. Wenkert, E. L. Michelotti, C. S. Swindell, *J. Am. Chem. Soc.* **101**, 2246 (1979).
18. E. Wenkert, E. L. Michelotti, C. S. Swindell, M. Tingoli, *J. Org. Chem.* **49**, 4894 (1984).
19. J. W. Dankwardt, *Angew. Chem. Int. Ed.* **43**, 2428 (2004).
20. B. T. Guan *et al.*, *Chem. Commun. (Camb.)* 1437 (2008).
21. M. Tobisu, T. Shimasaki, N. Chatani, *Angew. Chem. Int. Ed.* **47**, 4866 (2008).
22. J. A. Widegren, R. G. Finke, *J. Mol. Catal. A* **198**, 317 (2003).
23. Materials and methods are available as supporting material on *Science* Online.
24. We observed formation of cyclohexane and cyclohexene in the reaction of $Ni(COD)_2$ and PCy_3 with H_2 in the absence of diphenlyl ether under the same conditions (*23*).
25. F. Glorius, *Top. Organomet. Chem.* **21**, 1 (2007).
26. S. Díez-González, N. Marion, S. P. Nolan, *Chem. Rev.* **109**, 3612 (2009).
27. $Ni(COD)_2$ and PCy_3 were reported to catalyze silane-induced cleavage of polycyclic aromatic ethers (methoxynaphthalenes) and alkyl aryl ethers containing directing groups ortho to the C-O bond (*33*, *34*).
28. No reaction was observed in the absence of $Ni(COD)_2$, as shown through control experiments on the cleavage of 4-tert-butylbenzyl methyl ether with hydrogen in the presence of $AlMe_3$ (1 equiv.), SIPr·HCl (0.4 equiv.), and NaO^tBu (2.5 equiv.) in *m*-xylene at 120°C for 32 hours (*23*).
29. For example, heterogeneous hydrogenolysis of alkyl benzyl ethers proceeds selectively in the presence of diaryl ethers over $Pd(OH)_2/C$ (*35*).
30. K. Poppius, *Acta Chem. Scand. B* **38**, 611 (1984).
31. V. Snieckus, *Chem. Rev.* **90**, 879 (1990).
32. M. E. van der Boom, S. Y. Liou, Y. Ben-David, L. J. W. Shimon, D. Milstein, *J. Am. Chem. Soc.* **120**, 6531 (1998).
33. P. Álvarez-Bercedo, R. Martin, *J. Am. Chem. Soc.* **132**, 17352 (2010).
34. M. Tobisu, K. Yamakawa, T. Shimasaki, N. Chatani, *Chem. Commun.* Published online 24 January 2011 (10.1039/c0cc05169a).
35. B. A. Ellsworth *et al.*, *Bioorg. Med. Chem. Lett.* **18**, 4770 (2008).
36. We thank the BP for financial support of this project through the Energy Biosciences Program and T. Rauchfuss for helpful discussions. A provisional patent has been filed on the methods presented herein.

Supporting Online Material

www.sciencemag.org/cgi/content/full/332/6028/439/DC1
Materials and Methods
SOM Text
Figs. S1 to S3
Tables S1 to S6
References

15 November 2010; accepted 11 March 2011
10.1126/science.1200437

High-Performance Electrocatalysts for Oxygen Reduction Derived from Polyaniline, Iron, and Cobalt

Gang Wu,[1] Karren L. More,[2] Christina M. Johnston,[1] Piotr Zelenay[1]*

The prohibitive cost of platinum for catalyzing the cathodic oxygen reduction reaction (ORR) has hampered the widespread use of polymer electrolyte fuel cells. We describe a family of non–precious metal catalysts that approach the performance of platinum-based systems at a cost sustainable for high-power fuel cell applications, possibly including automotive power. The approach uses polyaniline as a precursor to a carbon-nitrogen template for high-temperature synthesis of catalysts incorporating iron and cobalt. The most active materials in the group catalyze the ORR at potentials within ~60 millivolts of that delivered by state-of-the-art carbon-supported platinum, combining their high activity with remarkable performance stability for non–precious metal catalysts (700 hours at a fuel cell voltage of 0.4 volts) as well as excellent four-electron selectivity (hydrogen peroxide yield <1.0%).

Thanks to the high energy yield and low environmental impact of hydrogen oxidation, the polymer electrolyte fuel cell (PEFC) represents one of the most promising energy conversion technologies available today. Of the many possible applications, ranging from sub-watt remote sensors to residential power generators in excess of 100 kW, automotive transportation is especially attractive. PEFCs promise major improvements over gasoline combustion, including better overall fuel efficiency and reduction in emissions (including CO_2). The spectacular progress in fuel cell technology notwithstanding, a large-scale market introduction of fuel cell–powered vehicles continues to face various challenges, such as the lack of hydrogen infrastructure and the technical issues associated with PEFC performance and durability under the operating conditions of an automotive power plant. The high cost of producing PEFCs represents the most formidable challenge and has driven much of the applied and fundamental fuel cell research in recent years.

According to the latest cost analysis, the fuel cell—more precisely, the fuel cell stack—is responsible for more than 50% of the PEFC power system cost (*1*, *2*). Although a state-of-the-art PEFC stack uses several high-priced components, the catalysts are by far the most expensive constituent, accounting for more than half of the stack cost. Because catalysts at both the fuel cell anode and cathode are based on platinum (Pt) or platinum alloys, their cost is directly linked to the price of Pt in the volatile and highly monopolized precious metal market. The precious metal catalyst is the only fuel cell stack component that will not benefit from economies of scale, and an increase in the demand for fuel cell power systems is bound to drive up the already high price of Pt, about $1830 per troy ounce at present ($2280 per troy ounce at its maximum in March 2008) (*3*). Thus, PEFCs are in need of efficient, durable, and inexpensive alternatives to Pt and Pt-based catalysts.

Ideally, Pt should be replaced at both fuel cell electrodes; however, its substitution at the cathode with a non–precious metal catalyst would have comparatively greater impact, because the slow oxygen reduction reaction (ORR) at this electrode requires much more Pt than the faster hydrogen oxidation at the anode. As a consequence, the development of non–precious metal catalysts with high ORR activity has recently become a major focus of PEFC research (*4*–*8*). The Pt replacement candidates that have attracted the most attention have been synthesized by heating precursors comprising nitrogen, carbon, and geologically abundant transition metals, iron and cobalt (M = Co and/or Fe) in particular (*9*–*14*). Although the nature of the active ORR catalytic sites in such N-M-C catalysts continues to be at the center of an ongoing debate (*6*, *7*, *10*, *15*), there is no doubt that the ORR performance of N-M-C catalysts strongly depends on the type of nitrogen and transition-metal precursors used, heat treatment temperature, carbon support morphology, and synthesis conditions.

We recently initiated a research effort to develop non–precious metal catalysts that combine high ORR activity with good performance stability, originally concentrating on materials obtained without heat treatment. The polypyrrole (PPy)-Co-C system prepared this way showed respectable performance durability for a non–precious metal

[1]Materials Physics and Applications Division, Los Alamos National Laboratory, Los Alamos, NM 87545, USA. [2]Materials Science and Technology Division, Oak Ridge National Laboratory, Oak Ridge, TN 37831, USA.

*To whom correspondence should be addressed. E-mail: zelenay@lanl.gov

catalyst, but its oxygen reduction activity remained relatively low (*5*). We then shifted toward high-temperature systems synthesized using predominantly iron, cobalt, and heteroatom polymer precursors (polypyrrole and polyaniline) (*16*, *17*). Such nitrogen-derived non–precious metal ORR catalysts have been under development for several decades, starting with the early work by Jasinski (*18*) and by Yeager and co-workers (*19*). Their research concentrated in particular on pyrolyzed transition metal–containing macrocycles and yielded catalysts that offered good ORR activity but suffered from poor stability in an acidic environment (*20*). The expensive macrocycles were later replaced in numerous studies by various combinations of nitrogen-containing compounds, transition-metal inorganic salts, and carbons, which ultimately led to considerable improvements in ORR activity but relatively little progress in stability. Polyaniline (PANI), which represents a favorable combination of aromatic rings connected via nitrogen-containing groups, was selected for this study as a promising template compound for nitrogen and carbon. Because of the similarity between the structures of PANI and graphite, the heat treatment of PANI could facilitate the incorporation of nitrogen-containing active sites into the partially graphitized carbon matrix. Furthermore, the use of such a polymer as a nitrogen precursor promised a more uniform distribution of nitrogen sites on the surface and an increase in the active-site density. In our effort, although several catalysts have shown promising oxygen reduction activity, only PANI-derived formulations appear to combine high ORR activity with unique performance durability for heat-treated non–precious metal catalysts. These catalysts are the subject of this report.

A schematic diagram describing the catalyst synthesis is shown in Fig. 1. In the approach used, a short-chain aniline oligomer was first mixed with high–surface area carbon material, pristine Ketjenblack EC-300J or modified Ketjenblack in the case of PANI-FeCo-C(2) (*21*), and transition metal precursors [cobalt(II) nitrate and/or iron(III) chloride], followed by the addition of $(NH_4)_2S_2O_8$ (ammonium persulfate, APS) as an oxidant to fully polymerize the aniline. After polymerization, water was evaporated from the suspension and the remaining solid phase was subjected to heat treatments in the range 400° to 1000°C under a N_2 atmosphere. The heat-treated product was then preleached in 0.5 M H_2SO_4 at 80° to 90°C for 8 hours to remove any unstable and ORR-nonreactive phases. The preleached catalyst then underwent a second heat treatment under N_2 as the final step of the synthesis (*21*).

The ORR activity and four-electron selectivity of various PANI-M-C catalysts and several control materials (as-received and heat-treated carbon, heat-treated metal-free PANI-C, and a 20 weight percent Pt/C reference catalyst) are shown in Fig. 2A. All experiments involving non–precious metal catalysts were carried out in 0.5 M H_2SO_4. The Pt/C reference catalyst was tested in 0.1 M $HClO_4$ to avoid performance loss caused by bisulfate adsorption, especially at higher electrode potentials (*22*). As established in previous research (*23*), at sufficiently high electrode overpotentials, carbon black alone can act as an oxygen reduction catalyst (mostly to H_2O_2 rather than H_2O; see Fig. 2A, plot 1). Although the high ORR overpotential on carbon can be lowered by a heat treatment alone (Fig. 2A, plot 2), a more substantial improvement in ORR activity, reflected by a shift in the onset ORR potential from 0.60 to 0.80 V (versus the reversible hydrogen electrode, RHE), is achieved after the addition of PANI (Fig. 2A, plot 3). Pyridinic, pyrrolic, and quaternary nitrogen centers are present in the heat-treated PANI-C sample (*24*). Nitrogen can be viewed in this case as an n-type carbon dopant that results in the formation of disordered carbon nanostructures and/or donates electrons to the carbon (*24*), thus facilitating the ORR (*25*). Iron or cobalt incorporation leads to a radical enhancement in the ORR activity and four-electron selectivity of the catalysts (Fig. 2A, plots 4 and 7). The ORR onset potential for the more active of the two PANI-FeCo-C catalysts and for the PANI-Fe-C catalyst is ~0.93 V (bottom part of Fig. 2A, plots 6 and 7, respectively). A rotating ring-disk electrode (RRDE) study additionally reveals very high selectivity of the PANI-derived catalysts for the four-electron reduction of oxygen. The H_2O_2 yield with PANI-Fe-C remains below 1% at all potentials, dropping to as low as 0.6% at 0.40 V. Unlike other non–precious metal catalysts, which show a peroxide yield in excess of 50% at lower loadings (*26*), the H_2O_2 yield measured with PANI-derived catalysts shows little loading dependence. Even at a low loading of 0.1 mg cm^{-2}, the H_2O_2 yield measured with the PANI-Fe-C catalyst is limited to a range of 0.6 to 3.8%, depending on electrode potential.

The disparity in the precious and non–precious metal catalyst loading notwithstanding, the performance gap between a state-of-the-art Pt/C (E-TEK) and PANI-Fe-C, expressed as a half-wave potential difference ($\Delta E_{1/2}$) in rotating disk electrode (RDE) testing, has been substantially reduced in this work to 43 mV relative to Pt/C at a "standard" loading of 20 μg_{Pt} cm^{-2} (Fig. 2A) and 59 mV relative to Pt/C at a "high" loading of 60 μg_{Pt} cm^{-2}.

Whereas cyclic voltammograms (CVs) of PANI-C and PANI-Co-C in N_2-saturated H_2SO_4 solution are virtually featureless, the CV of PANI-Fe-C reveals a pair of well-developed redox peaks at ~0.64 V (fig. S1). The full width at half maximum (FWHM) of these peaks is ~100 mV, which is very close to the theoretical value of 96 mV expected for a reversible one-electron process involving surface species (*27*). There are two surface processes that can possibly give rise to the observed redox behavior in this case: (i) one-electron reduction/oxidation of the surface quinone/hydroquinone groups (*28*), and (ii) Fe^{3+}/Fe^{2+}

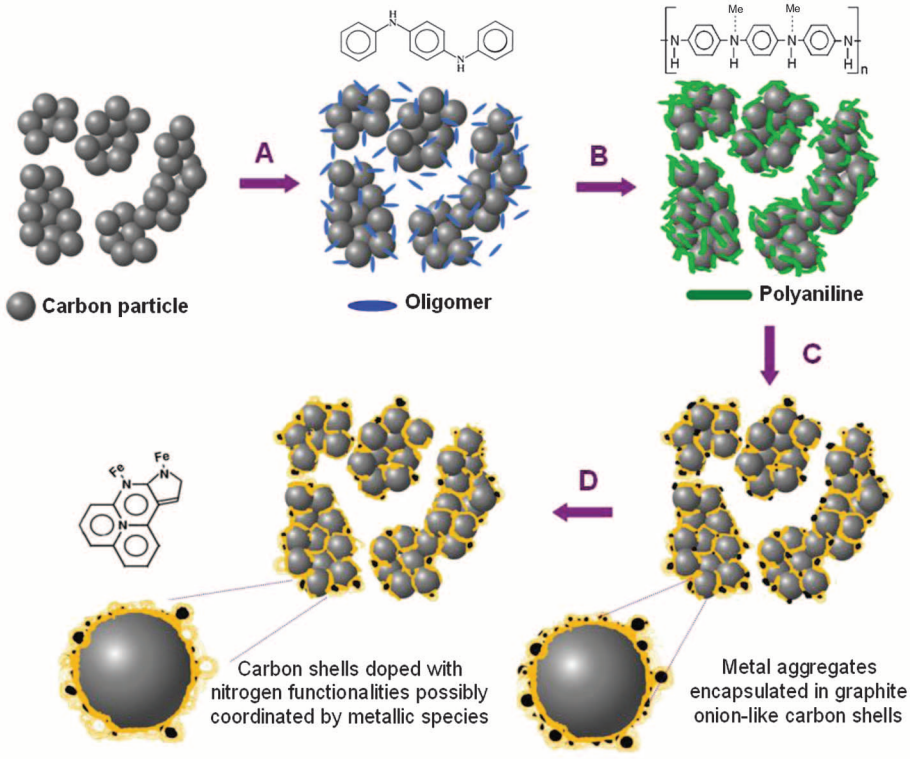

Fig. 1. Schematic diagram of the synthesis of PANI-M-C catalysts. (**A**) Mixing of high–surface area carbon with aniline oligomers and transition-metal precursor (M: Fe and/or Co). (**B**) Oxidative polymerization of aniline by addition of APS. (**C**) First heat treatment in N_2 atmosphere. (**D**) Acid leaching. The second heat treatment after acid leach is not shown.

reduction/oxidation. In support of the latter reaction, an in situ electrochemical x-ray absorption study of the PANI-Fe-C system shows a correlation between the change in the oxidation state of Fe species in the catalysts and the potential of the reversible CV feature in the PANI-Fe-C catalyst voltammetry (*17*).

Additional kinetic data (fig. S2 and table S1) reveal differences in the Tafel slope of oxygen reduction on the different catalysts studied in this work. A Tafel slope of 67 mV decade^{-1} was measured for PANI-Co-C—a much lower value than the Tafel slope of 87 mV decade^{-1} obtained for PANI-Fe-C. The rate-determining step of the ORR for the latter catalyst is likely to simultaneously involve the migration of reaction intermediates and charge transfer. The exchange current density (i_0) is nearly two orders of magnitude higher for the PANI-Fe-C catalyst (4×10^{-8} A cm^{-2}) than for PANI-Co-C (5×10^{-10} A cm^{-2}). Together with the differences in the onset potential of oxygen reduction (*21*), the Tafel slope (mass transport–corrected), and four-electron selectivity (Fig. 2A) already described, the disparity of two orders of magnitude in the i_0 value for the two catalysts implies that the ORR-active sites and reaction mechanisms are likely different in both cases. Ex situ x-ray absorption analysis provides evidence for a different chemical environment in each case. Cobalt coordination in the PANI-Co-C catalyst appears to closely resemble that in Co_9S_8, with the dominant x-ray absorption fine structure (XAFS) peak between 2 to 3 Å consistent with a known Co-Co shell (*29*). XAFS of the PANI-Fe-C catalyst shows a peak at ~1.50 Å, which is indicative of coordination to a lighter element (either N or O) at a much shorter distance than nearest neighbors in metallic Fe (XAFS peak at ~2.2 Å) or in FeN_4-type structures in Fe macrocycles (~1.63 Å) (*30*).

In catalyst synthesis chemistry, the heat treatment temperature is a major factor in inducing catalytic activity of PANI-derived catalysts and assuring performance stability. We used an RDE to study the ORR activity of a PANI-Fe-C catalyst as a function of the heat treatment temperature in the range 400° to 1000°C. RDE studies were conducted at room temperature and in 0.5 M H_2SO_4 electrolyte (Fig. 2B). The performance of the catalyst synthesized by heat treatment at 400°C is very similar to that of Ketjenblack itself (bottom part of Fig. 2A, plot 1). The activity, as measured by the ORR onset and half-wave potentials ($E_{½}$) in the RDE polarization plots, increases upon raising the heat treatment temperature up to 900°C and then drops for catalysts synthesized at even higher temperatures. The H_2O_2 yield measured for the best-performing PANI-Fe-C catalyst, heat treated at 900°C, is below 1% over the potential range from 0.1 to 0.8 V versus RHE, signaling virtually complete reduction of O_2 to H_2O in a four-electron process. This avoidance of the much less efficient, and therefore undesirable, two-electron reaction to peroxide matches, and possibly exceeds, the four-electron selectivity of Pt-based catalysts (3 to 4% H_2O_2 yield at 0.4 V on 14 μg_{Pt} cm^{-2} Pt/C) (*31*).

We next conducted extensive physical characterization to obtain a structural explanation for the correlation of the ORR activity of the catalysts with the heat treatment temperature. Fourier transform infrared (FTIR) spectra of PANI-Fe-C (fig. S3) show that between 400° and 600°C the benzene-type (1100 cm^{-1}) and quinone-type (1420 cm^{-1}) structures (*32*) on the main PANI chain break into smaller fragments, such as C=N (1300 cm^{-1}), which may be precursor states for ORR-active sites. The latter finding corresponds with scanning electron microscopy (SEM) results (fig. S4) indicating that in this range of heat treatment temperatures, PANI starts to lose its characteristic nanofibrous structure (fibers ~40 nm in diameter and ~200 nm in length) and gradually converts into more spherical particles. The carbon structure becomes more graphitic during the heat treatment at 900°C (HRTEM inset in fig. S4) (see below). After the treatment at an even higher temperature of 1000°C, the particle morphology becomes highly nonuniform, a change accompanied by a substantial surface area loss, as determined using Brunauer-Emmet-Teller (BET) technique.

The fuel cell polarization and stability plots for PANI-derived catalysts are shown in Fig. 3. In good agreement with electrochemical measurements, the addition of transition metals leads to a considerable activity enhancement of the catalysts relative to the metal-free PANI-C (Fig. 3A). Also in agreement with the RDE data in Fig. 2A, PANI-Fe-C exhibits higher ORR activity than PANI-Co-C. The best-performing catalyst in fuel cell testing, with an excellent combination of high ORR activity and long-term performance durability, is the more active of the two FeCo mixed-metal materials, PANI-FeCo-C(2). This catalyst

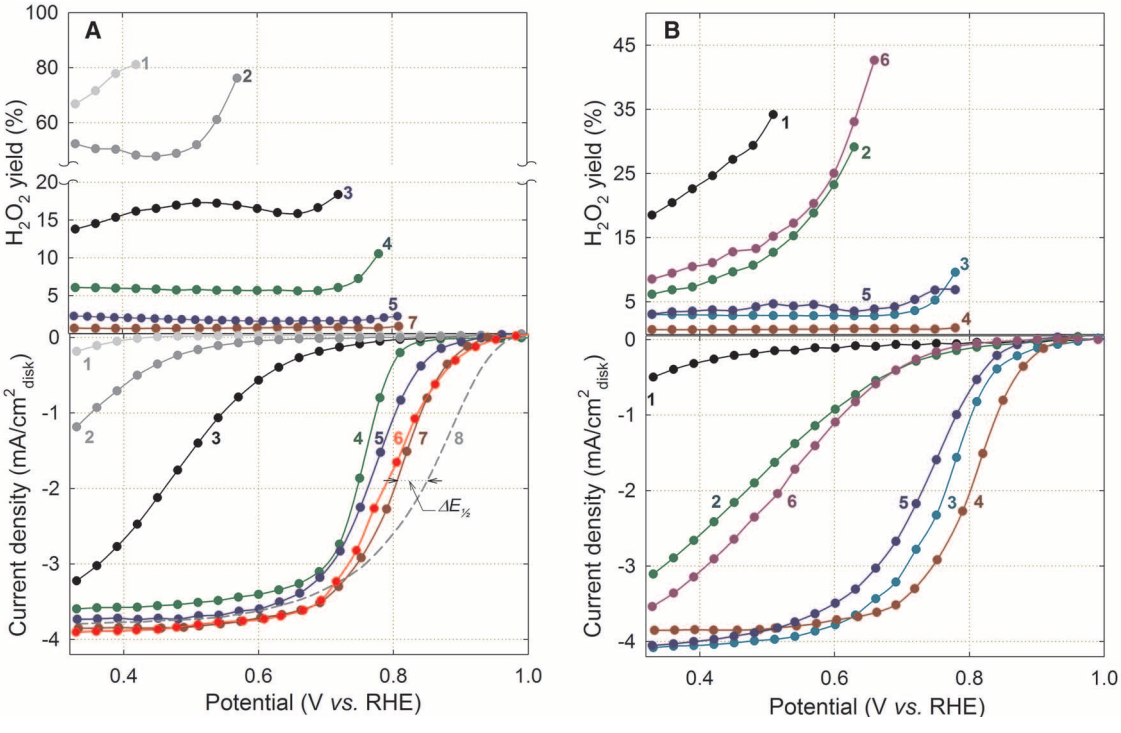

Fig. 2. (**A**) Steady-state ORR polarization plots (bottom) and H_2O_2 yield plots (top) measured with different PANI-derived catalysts and reference materials: 1, as-received carbon black (Ketjenblack EC-300J); 2, heat-treated carbon black; 3, heat-treated PANI-C; 4, PANI-Co-C; 5, PANI-FeCo-C(1); 6: PANI-FeCo-C(2); 7, PANI-Fe-C; 8, E-TEK Pt/C (20 μg_{Pt} cm^{-2}). Electrolyte: O_2-saturated 0.5 M H_2SO_4 [0.1 M $HClO_4$ in experiment involving Pt catalysts (dashed line)]; temperature, 25°C. RRDE experiments were carried out at a constant ring potential of 1.2 V versus RHE. RDE/RRDE rotating speed, 900 rpm; non–precious metal catalyst loading, 0.6 mg cm^{-2}. (**B**) Steady-state ORR polarization plots (bottom) and H_2O_2 yield plots (top) measured with a PANI-Fe-C catalyst in 0.5 M H_2SO_4 electrolyte as a function of the heat treatment temperature: 1, 400°C; 2, 600°C; 3, 850°C; 4, 900°C; 5, 950°C; 6, 1000°C.

also shows the highest RDE activity, matched only by PANI-Fe-C (see low current-density range in Fig. 2A, plots 6 and 7), as well as the highest maximum power density: 0.55 W cm^{-2}, reached at 0.38 V. Unlike PANI-Fe-C, the mixed-metal catalysts maintain their high ORR activity when combined with Nafion ionomer in a fuel cell–type electrode under operation in the highly acidic environment of the fuel cell cathode, thus reflecting better stability of the PANI-FeCo-C catalyst (see below). The open-cell voltage (OCV) of a hydrogen fuel cell operated with Fe-containing

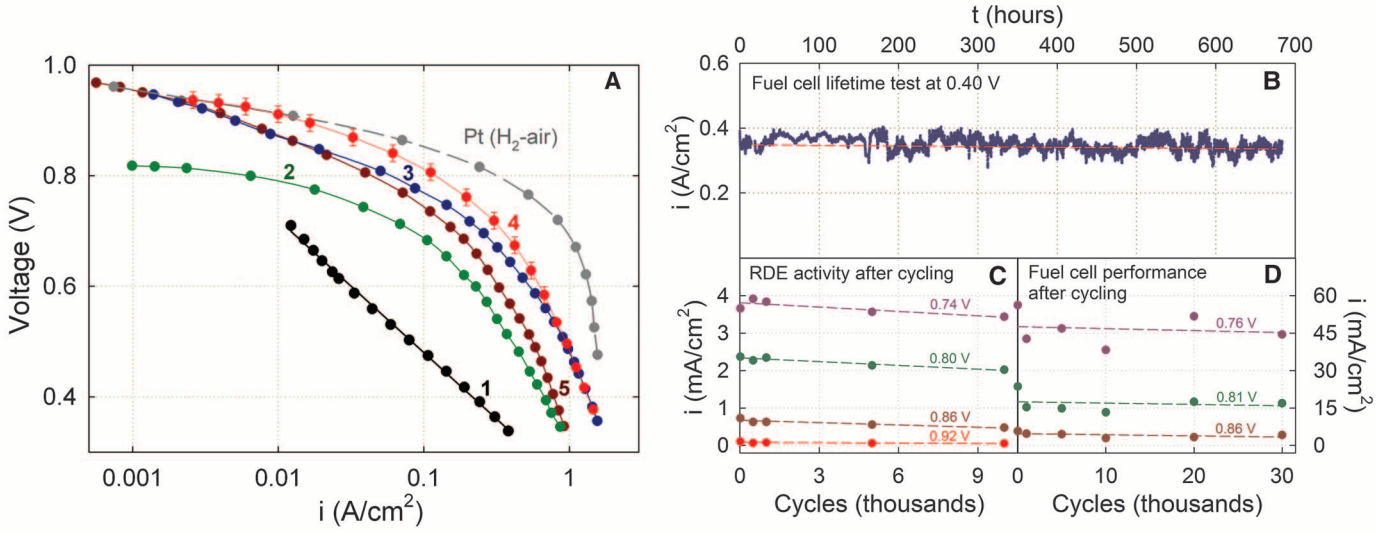

Fig. 3. Fuel cell and performance durability testing. (**A**) H_2-O_2 fuel cell polarization plots recorded with various PANI-derived cathode catalysts at a loading of ~4 mg cm^{-2}: 1, PANI-C; 2, PANI-Co-C; 3, PANI-FeCo-C(1); 4, PANI-FeCo-C(2) (SDs from three independent measurements marked for all data points); 5, PANI-Fe-C. Performance of an H_2-air fuel cell with a Pt cathode (0.2 mg_{Pt} cm^{-2}) is shown for comparison (dashed line). All tests used a Pt/C catalyst at a loading of 0.25 mg_{Pt} cm^{-2} at the anode; anode and cathode gas pressure, 2.8 bar. (**B**) Long-term stability test of a PANI-FeCo-C(1) catalyst at a constant fuel cell voltage of 0.40 V (2.8 bar H_2/2.8 bar air; 0.25 mg_{Pt} cm^{-2} anode; cell temperature 80°C). (**C**) PANI-Fe-C catalyst RDE performance at various potentials after potential cycling in nitrogen between 0.6 and 1.0 V in 0.5 M H_2SO_4 (catalyst loading, 0.6 mg cm^{-2}). (**D**) PANI-Fe-C catalyst H_2-O_2 fuel cell performance at various voltages after voltage cycling in nitrogen between 0.6 and 1.0 V (cathode catalyst loading, 2.0 mg cm^{-2}, Pt/C anode catalyst loading, 0.25 mg_{Pt} cm^{-2}; anode and cathode gas pressure, 1.0 bar).

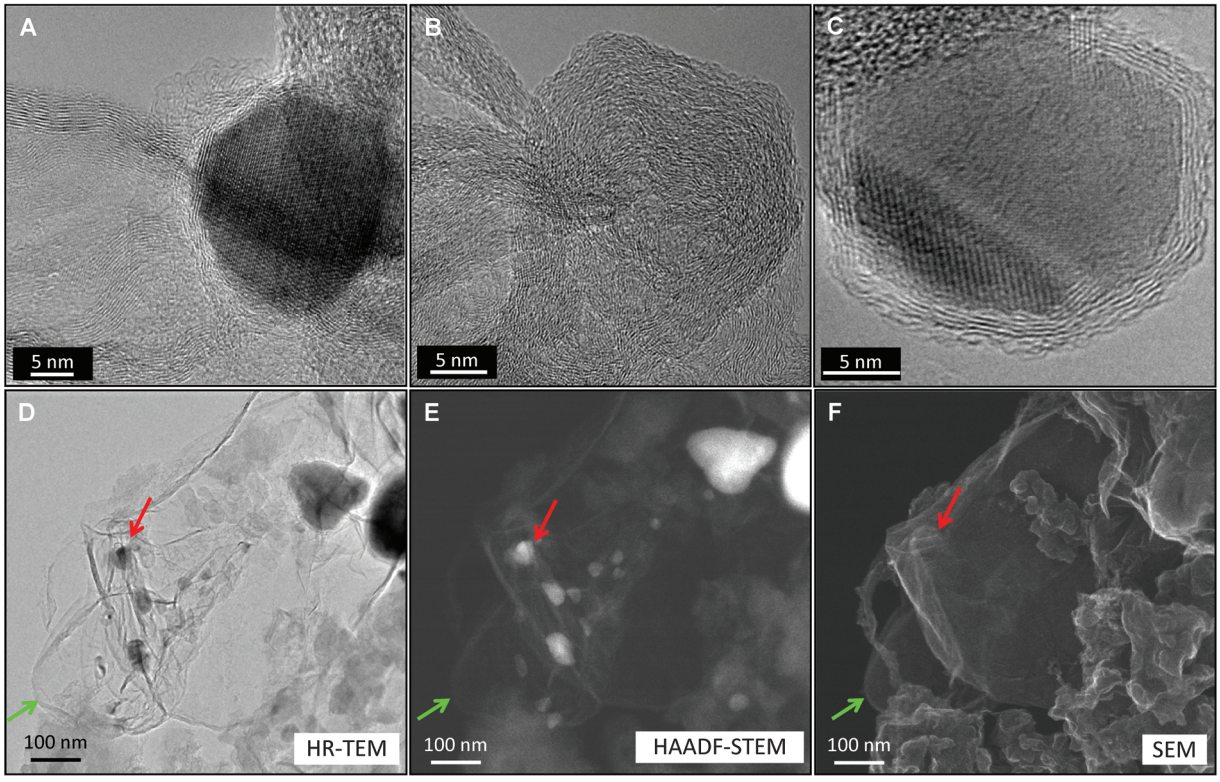

Fig. 4. Micrographs of a PANI-FeCo-C(1) catalyst. (**A**) HRTEM image of a typical non–precious metal catalyst nanostructure involving carbon nanofibers and metal-aggregates incorporated in graphitic nanoshells. (**B**) HRTEM image of hollow nanoshells. (**C**) HRTEM image of onion-like nanoshells. (**D** to **F**) HRTEM, HAADF-STEM, and SEM images of the same localized region in an area exhibiting a graphene sheet–like structure, where the green arrows designate the layered graphene sheet in each image and the red arrows designate the same FeCo-containing nanoparticle (technique used is noted in each micrograph).

PANI-derived catalysts is ~0.90 V with an air-operated cathode and ~0.95 V with a cathode operated on pure oxygen. The OCV value remains unchanged for more than 100 hours in the H_2-air fuel cell (*17*).

A 700-hour fuel-cell performance test at a constant cell voltage of 0.4 V reveals very promising performance stability of the PANI-FeCo-C(1) catalyst at the fuel cell cathode. The cell current density in a lifetime test (Fig. 3B) remains nearly constant at ~0.340 A cm^{-2}. The current density declines by only 3%, from the average value of 0.347 A cm^{-2} in the first 24 hours to 0.337 A cm^{-2} in the last 24 hours of the test (average current-density loss, 18 μA $hour^{-1}$). Fuel cell performance durability (Fig. 3B) represents a substantial improvement over the durability recently reported by the Dodelet group (*6*). The initially very active catalyst in the latter work suffered from fast performance deterioration, losing ~38% of activity during 100 hours of H_2-air testing at 0.40 V. Although quite durable by the standards of non–precious metal ORR catalysts, both PANI-Fe-C and PANI-Co-C are less stable than PANI-FeCo-C(1), incurring performance losses of ~90 and 130 μA $hour^{-1}$, respectively. A stabilizing role of Co in the binary catalyst is a distinct possibility.

The high stability of the PANI-derived catalysts does not apply solely to constant-potential operation of an RDE (nor to constant-voltage operation of a fuel cell); it extends over potential-cycling conditions, and hence it is especially relevant to practical fuel cell systems. High cycling stability of a PANI-Fe-C catalyst at various RDE potentials and fuel cell voltages is demonstrated in Fig. 3, C and D, respectively (see also fig. S5). The cycling was carried out within a potential (RDE) and voltage (fuel cell) range of 0.6 to 1.0 V in nitrogen gas at a scan rate of 50 mV s^{-1} (a protocol recommended by the U.S. automotive industry). The catalyst performance loss calculated from linear regression was 10 to 39% after 10,000 RDE cycles (Fig. 3C) and 3 to 9% after 30,000 fuel cell cycles (Fig. 3D), further attesting to the high durability of PANI-derived catalysts, especially in the fuel cell cathode.

The morphology of the highly ORR-active and durable PANI-FeCo-C(1) catalyst before and after the heat treatment at 900°C (followed by acid leaching) is depicted by the SEM images in fig. S6. In this catalyst, as in PANI-Fe-C, the PANI nanofibers are replaced by a highly graphitized carbon phase during heat treatment. High-resolution transmission electron microscopy (HRTEM) and high-angle annular dark-field scanning TEM (HAADF-STEM) images of the PANI-FeCo-C(1) catalyst heat-treated at 900°C are shown in Fig. 4 and attest to the presence of diverse carbon nanostructures, also highlighted in HRTEM images in figs. S7 and S8. Metal-containing particles are to a large extent encapsulated in well-defined onion-like graphitic carbon nanoshells (Fig. 4, A and C). Such a well-defined graphitized carbon shell surrounding metal-rich particles was previously observed with iron(III) tetramethoxyphenyl porphyrin chloride (FeTMPP-Cl) when the heat treatment temperature was raised to 1000°C (*33*). In the latter work, the graphite shell formation was correlated to an increase in the catalyst open-circuit potential in oxygen-saturated solution. Carbon nanosheets grown over the metal particles are also observed in Fig. 4, A and B. In some cases, the metallic cobalt and/or iron sulfide phases (*16*) within the graphite-coated particles can be removed by acid leaching, leaving behind hollow and onion-like carbon nanoshells that are easily observable by HRTEM (Fig. 4B).

The carbon structure formed during the heat treatment, rather than being ideally graphitic, is somewhat disordered (e.g., turbostratic or mesographitic). This lattice distortion within the *c*-planes is reflected by a larger d-spacing of the (002) basal planes in the carbon relative to that in a well-ordered structure of graphite (*34*). The measured (002) d-spacing, ranging from ~0.34 to 0.36 nm, may facilitate incorporation of nitrogen into the graphitic structure and thereby enhance the number of active sites. The formation of graphene sheets appears to be closely associated with the improved durability of PANI-derived catalysts. A substantial fraction of multilayered graphene sheets in the catalyst are colocated with the particles of $Fe(Co)S_x$, as shown by the green and red arrows, respectively, in the complementary TEM, HAADF-STEM, and SEM images acquired from the same location in Fig. 4, D to F, respectively. Apart from likely contributing to active-site formation, the graphitization of the onion-like nanoshells and nanofibers as well as the presence and formation of graphene sheets throughout the PANI-derived catalysts may also enhance the electronic conductivity and corrosion resistance of the carbon-based catalysts (*35*, *36*). The presence of the graphitized carbon phase in an active catalyst deserves further study, as such a phase may play a role in hosting ORR-active sites and enhancing stability of the PANI-derived catalysts.

Bridging the remaining performance gap in intrinsic activity and durability between non–precious metal catalysts and platinum in PEFCs will require determination of the active oxygen reduction site and a better understanding of the reaction mechanism.

References and Notes

1. B. James, J. Kalinoski, in *DOE-EERE Fuel Cell Technologies Program—2009 DOE Hydrogen Program Review* (www.hydrogen.energy.gov/pdfs/review09/fc_30_james.pdf).
2. J. Sinha, S. Lasher, Y. Yang, in *DOE-EERE Fuel Cell Technologies Program—2009 DOE Hydrogen Program Review* (www.hydrogen.energy.gov/pdfs/review09/fc_31_sinha.pdf).
3. Johnson Matthey (www.platinum.matthey.com/pgm-prices/price-charts).
4. R. Borup *et al.*, *Chem. Rev.* **107**, 3904 (2007).
5. R. Bashyam, P. Zelenay, *Nature* **443**, 63 (2006).
6. M. Lefèvre, E. Proietti, F. Jaouen, J. P. Dodelet, *Science* **324**, 71 (2009).
7. C. M. Johnston, P. Piela, P. Zelenay, in *Handbook of Fuel Cells: Fundamentals, Technology, and Applications*, W. Vielstich, H. A. Gasteiger, H. Yokokawa, Eds. (Wiley, Chichester, UK, 2009), vol. 5, pp. 48–70.
8. F. Jaouen *et al.*, *Energy Environ. Sci.* **4**, 114 (2011).
9. S. Maldonado, K. J. Stevenson, *J. Phys. Chem. B* **108**, 11375 (2004).
10. P. H. Matter, L. Zhang, U. S. Ozkan, *J. Catal.* **239**, 83 (2006).
11. R. Kothandaraman, V. Nallathambi, K. Artyushkova, S. C. Barton, *Appl. Catal. B* **92**, 209 (2009).
12. U. I. Koslowski, I. Abs-Wurmbach, S. Fiechter, P. Bogdanoff, *J. Phys. Chem. C* **112**, 15356 (2008).
13. F. Jaouen *et al.*, *ACS Appl. Mater. Interfaces* **1**, 1623 (2009).
14. T. Ikeda *et al.*, *J. Phys. Chem. C* **112**, 14706 (2008).
15. V. Nallathambi, J. W. Lee, S. P. Kumaraguru, G. Wu, B. N. Popov, *J. Power Sources* **183**, 34 (2008).
16. G. Wu, Z. W. Chen, K. Artyushkova, F. H. Garzon, P. Zelenay, *ECS Trans.* **16**, 159 (2008).
17. G. Wu *et al.*, *ECS Trans.* **25**, 1299 (2009).
18. R. Jasinski, *Nature* **201**, 1212 (1964).
19. S. Gupta, D. Tryk, I. Bae, W. Aldred, E. Yeager, *J. Appl. Electrochem.* **19**, 19 (1989).
20. J. P. Dodelet, in *N_4-Macrocyclic Metal Complexes*, J. H. Zagal, F. Bedioui, J. P. Dodelet, Eds. (Springer, New York, 2006), pp. 83–147.
21. See supporting material on *Science* Online.
22. S. Thomas, Y. E. Sung, H. S. Kim, A. Wieckowski, *J. Phys. Chem. C* **100**, 11726 (1996).
23. H. Wang, R. Cote, G. Faubert, D. Guay, J. P. Dodelet, *J. Phys. Chem. B* **103**, 2042 (1999).
24. G. Wu, D. Y. Li, C. S. Dai, D. L. Wang, N. Li, *Langmuir* **24**, 3566 (2008).
25. V. V. Strelko *et al.*, *Surf. Sci.* **548**, 281 (2004).
26. A. Bonakdarpour *et al.*, *Electrochem. Solid-State Lett.* **11**, B105 (2008).
27. E. Laviron, *J. Electroanal. Chem.* **52**, 395 (1974).
28. K. Kinoshita, J. A. S. Bett, *Carbon* **11**, 403 (1973).
29. V. Schwartz, R. Prins, X. Wang, W. M. H. Sachtler, *J. Phys. Chem. B* **106**, 7210 (2002).
30. J. Yang, D.-J. Liu, N. N. Kariuki, L. X. Chen, *Chem. Commun. (Camb.)* (3): 329 (2008).
31. M. Inaba, H. Yamada, J. Tokunaga, A. Tasaka, *Electrochem. Solid-State Lett.* **7**, A474 (2004).
32. M. Baibarac, I. Baltog, S. Lefrant, J. Y. Mevellec, O. Chauvet, *Chem. Mater.* **15**, 4149 (2003).
33. S. L. Gojković, S. Gupta, R. F. Savinell, *J. Electrochem. Soc.* **145**, 3493 (1998).
34. J. Zheng, T. C. Ekstrom, S. K. Gordeev, M. Jacob, *J. Mater. Chem.* **10**, 1039 (2000).
35. W. M. Zhang, P. Sherrell, A. I. Minett, J. M. Razal, J. Chen, *Energy Eviron. Sci.* **3**, 1286 (2010).
36. F. Hasché, M. Oezaslan, P. Strasser, *Phys. Chem. Chem. Phys.* **12**, 15251 (2010).

37. We thank R. Adzic, Y. S. Kim, J. Chlistunoff, F. Garzon, R. Mukundan, H. Chung, and S. Conradson for stimulating discussions. Supported by the Energy Efficiency and Renewable Energy Office of the U.S. Department of Energy (DOE) through the Fuel Cell Technologies Program, and by Los Alamos National Laboratory through the Laboratory-Directed Research and Development Program. Microscopy research was supported by the Oak Ridge National Laboratory's SHaRE User Facility, sponsored by the DOE Office of Basic Energy Sciences. The authors have filed a patent through Los Alamos National Laboratory on the catalysts described herein.

Supporting Online Material

www.sciencemag.org/cgi/content/full/332/6028/443/DC1
Materials and Methods
Table S1
Figs. S1 to S8
References

23 November 2010; accepted 24 March 2011
10.1126/science.1200832